Magnetotransport Properties of Graphene Nanoribbons with Zigzag Edges

Shuang Wu,[1,4,*] Bing Liu,[1,4] Cheng Shen,[1,4] Si Li,[2] Xiaochun Huang,[1,4] Xiaobo Lu,[1,4] Peng Chen,[1,4] Guole Wang,[1,4] Duoming Wang,[1,4] Mengzhou Liao,[1,4] Jing Zhang,[1,4] Tingting Zhang,[1,4] Shuopei Wang,[1,4] Wei Yang,[1,4] Rong Yang,[1,4] Dongxia Shi,[1,4] Kenji Watanabe,[3] Takashi Taniguchi,[3] Yugui Yao,[2] Weihua Wang,[1,4] and Guangyu Zhang[1,4,5,6,†]

[1]*Institute of Physics, Chinese Academy of Sciences, Beijing 100190, China*
[2]*School of Physics, Beijing Institute of Technology, Beijing 100081, China*
[3]*National Institute for Materials Science, 1-1 Namiki, Tsukuba 305-0044, Japan*
[4]*School of Physical Sciences, University of Chinese Academy of Sciences, Beijing 100190, China*
[5]*Collaborative Innovation Center of Quantum Matter, Beijing 100190, China*
[6]*Beijing Key Laboratory for Nanomaterials and Nanodevices, Beijing 100190, China*

(Received 17 November 2017; published 22 May 2018)

The determination of the electronic structure by edge geometry is unique to graphene. In theory, an evanescent nonchiral edge state is predicted at the zigzag edges of graphene. Up to now, the approach used to study zigzag-edged graphene has mostly been limited to scanning tunneling microscopy. The transport properties have not been revealed. Recent advances in hydrogen plasma-assisted "top-down" fabrication of zigzag-edged graphene nanoribbons (Z-GNRs) have allowed us to investigate edge-related transport properties. In this Letter, we report the magnetotransport properties of Z-GNRs down to ~70 nm wide on an *h*-BN substrate. In the quantum Hall effect regime, a prominent conductance peak is observed at Landau $\nu = 0$, which is absent in GNRs with nonzigzag edges. The conductance peak persists under perpendicular magnetic fields and low temperatures. At a zero magnetic field, a nonlocal voltage signal, evidenced by edge conduction, is detected. These prominent transport features are closely related to the observable density of states at the hydrogen-etched zigzag edge of graphene probed by scanning tunneling spectroscopy, which qualitatively matches the theoretically predicted electronic structure for zigzag-edged graphene. Our study gives important insights for the design of new edge-related electronic devices.

DOI: 10.1103/PhysRevLett.120.216601

A peculiar aspect of a finite-sized graphene sheet is that its electronic properties strongly depend on the edge configuration [1], especially when its physical dimensions are reduced to the nanometer scale [2,3]. A nondispersive single-electron band localized near the zigzag edge exists, hosting the so-called "edge states," with energies at or close to the Dirac point [4–6]. Most often, these localized edge states are predicted to have exotic properties, leading to edge magnetism [7], spin ordered state-induced gap opening [8], and charge accumulation at the edges in the quantum Hall effect [6,9], to mention a few.

Thus far, zigzag-edged graphene has been mostly probed by scanning tunneling microscopy (STM) on cleaved or STM-tip cut graphite and "bottom-up" chemically synthesized samples [10–13]. However, in terms of transport studies, device fabrication is a bottleneck for these zigzag-edged graphene materials on conductive substrates. Additionally, graphene nanostructures fabricated by standard top-down fabrication techniques [*e*-beam lithography (EBL) and etching, e.g., oxygen plasma etching] exhibit disordered edges; thus, the electrical transport properties for a zigzag-edged graphene structure are sparsely reported. To obtain well-defined zigzag edges via a top-down fabrication process, the etching has to be anisotropic within graphene basal plane [14,15]. In this study, we investigate the magnetotransport properties of monolayer zigzag-edged graphene nanoribbons fabricated using hydrogen-plasma anisotropic etching on hexagonal boron nitride (*h*-BN) substrates.

To characterize the atomic structure of the etched edge of graphene, we first carried out hydrogen-plasma etching for epitaxial graphene on a conductive 6*H*-SiC(0001) substrate (heavily *n* doped) [16]. Hexagonal pits enlarged from the defects in graphene can be found after anisotropic etching [15,17,18]. A typical one is shown in Fig. 1(a). Based on reported results [19,20], as well as the enlarged STM topography of the etched graphene edge with atomic resolution [Fig. 1(b)], we can distinguish edges that are dominated by zigzag orientation and hydrogen terminated. The edge consists of zigzag segments (each segment is several nanometers long), with one or two atomic steps showing. Predominantly zigzag segments are expected to preserve the zigzag edge property [10]. The hexagonal bulk graphene lattice, together with a $(\sqrt{3} \times \sqrt{3})R30°$ superstructure near the edge, is clearly resolved in Fig. 1(b) and verified by the fast Fourier transformation (FFT) image [inset in Fig. 1(b)] [20–23].

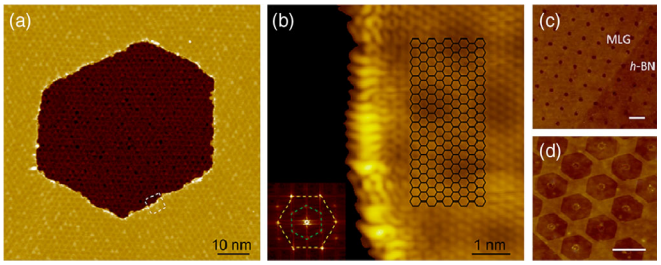

FIG. 1. STM images of the hydrogen-plasma etched graphene on 6H-SiC(0001) and atomic force microscopy (AFM) images of Z-GNRs on h-BN before and after hydrogen-plasma etching. (a) STM overview ($V_s = -1.0$ V,$I = 100$ pA,$T = 4.9$ K) of the etched graphene, showing an intact hexagonal pit. (b) Englarged STM image ($V_s = -500$ mV, $I = 300$ pA, $T = 4.9$ K) of the dotted area in (a). The black superimposed graphene lattice shows that the etched edge is predominantly in a zigzag orientation. Inset shows the FFT image of the top-layer graphene near the edge, where bulk graphene lattice and the $(\sqrt{3} \times \sqrt{3})R30°$ superstructure are highlighted by yellow and green hexagons, respectively. (c) AFM image of circular dot patterns in MLG on h-BN created by EBL and oxygen-plasma etching. The scale bar is 500 nm. (d) AFM image of hydrogen-plasma etched hexagonal hole arrays in graphene on h-BN. The scale bar is 500 nm.

We then fabricated a zigzag-edged graphene nanoribbon on an h-BN substrate for a transport study. Both monolayer graphene and multilayer-layer h-BN were produced via mechanical cleavage. Graphene/h-BN-stacked structures were fabricated through a dry transfer process [16]. We chose the h-BN substrate because it is chemical inert, atomically flat and smooth, resulting in less charged impurity scattering and higher carrier mobility [24,25]. Similar to the hydrogen-etched hexagonal pits in graphene on 6H-SiC(0001), circular dots in monolayer graphene (MLG) on h-BN [Fig. 1(c)], created by EBL and oxygen-plasma etching [14,16,26], are enlarged into hexagonal holes by anisotropic etching [Fig. 1(d)]. In between two parallel hexagonal holes, a zigzag-edged graphene nanoribbon (Z-GNR) is fabricated. In addition to the atomic structure of the edge probed by STM, the high quality of the Z-GNRs can be characterized by Raman spectroscopy, Fig. S1 in the Supplemental Material [16].

As-fabricated Z-GNRs show predominantly zigzag edges terminated with hydrogen, as discussed above. These well-defined Z-GNRs thus allow us to investigate their edge-related magnetotransport properties. Here we focus on those Z-GNRs with a width ranging from 60 to 120 nm to avoid drastically decreased carrier mobility or the Coulomb blockade effect [27,28].

Figure 2(a) shows a schematic illustration of the two-terminal Z-GNR device for transport measurements. The magnetotransport properties of a typical Z-GNR device (sample #t116) with a channel length of $l \sim 240$ nm and a width of $w \sim 68$ nm were shown in Fig. 2(b), illustrating the Landau fan diagram for G as a function of V_g and B. We can clearly label the filling factor $\nu = 1, 0, -2, -6$ in the Landau fan diagram according to the quantized Hall conductance.

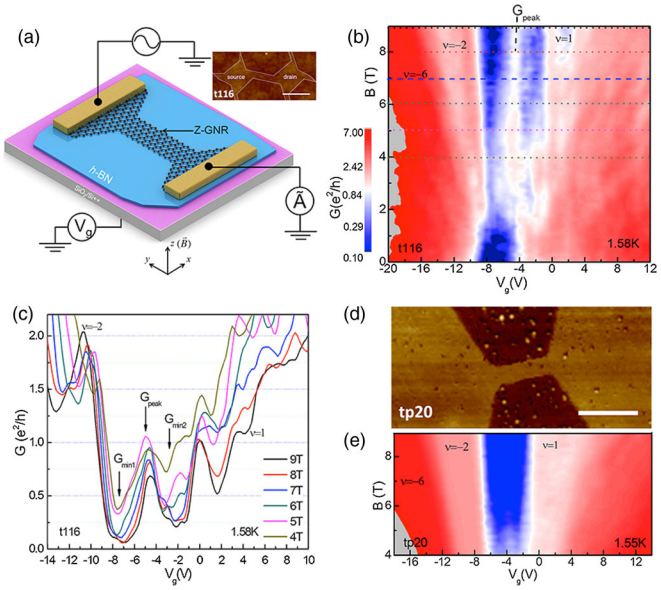

FIG. 2. Magnetotransport of the Z-GNR device. (a) Schematic diagram of a Z-GNR device with two terminals. A typical Z-GNR/h-BN device with width ~68 nm shown as inset AFM (scale bar is 300 nm). (b) Landau fan diagram G(V_g, B). (c) The typical transfer curves at several B from a (~3 kΩ contact resistance was subtracted). (d) The AFM image of a control sample#tp20. The scale bar is 300 nm. (e) Landau fan diagram of sample#tp20 G(V_g, B). Color scale is the same as Fig. 2(b).

Unlike the recently reported two-terminal quantum Hall effect (QHE) profile of GNRs [29,30], we can observe a nontrivial conductance peak ($V_g \approx -5$ V) persistently in the middle of $\nu = 0$ regime at $B > 4$ T. The detailed evolution for the conductance peak as well as the $\nu = 0$ states for varying B is extracted and plotted in Fig. 2(c). In the Landau filling regime, we labeled the conductance peak and conductance valleys on both sides as G_{peak}, $G_{\text{min}\,1}$, and $G_{\text{min}\,2}$, respectively. This additional peak is also observed in other Z-GNR devices (Fig. S2) [16] but is absent in the control sample, such as the edge-disordered GNR with $l \sim 260$ nm and $w \sim 86$ nm [sample #tp20, Fig. 2(d)] fabricated by a standard oxygen-plasma-etching based fabrication process. Note that oxygen plasma etches graphene and h-BN isotropically and the etched edge is random oriented (Fig. S3) [16,31]. Since the sample aspect ratio $l/w > 1$, we can rule out that this additional conductance peak at Landau filling $\nu = 0$ originates from the deformed quantized Hall plateaus caused by the size effect [32,33]. For the control sample, the minimum conductance at Landau filling $\nu = 0$ is labeled $G_{\text{min\_tp20}}$. In the QHE regime, $G_{\text{min}\,1}$, $G_{\text{min}\,2}$, and $G_{\text{min\_tp20}}$ decrease significantly with increasing B, which indicates the existence of a $\nu = 0$ bulk state. However, the magnitude of the G_{peak} located in the gapped $\nu = 0$ state shows little change. Moreover, the position of G_{peak} remains unchanged, which is different from the shift in the position of quantized Hall conductance observed for increasing magnetic field.

Although the quantum Hall effect is universal among GNR devices, the additional conductance peak can only be observed in high quality Z-GNR devices.

To further investigate the transport properties of this $\nu = 0$ conductance peak, we performed a series of measurements at different temperatures under a certain fixed magnetic field, e.g., $B = 9$ T [Fig. 3(a)]. Similar measurements were also performed for the control sample, with the data shown in Fig. 3(b). The G_{peak}, $G_{\mathrm{min}\,1}$, $G_{\mathrm{min}\,2}$ values for sample#116 and the $G_{\mathrm{min\_tp20}}$ value for sample#tp20 as a function of inverse temperature $(1/T)$ are extracted and plotted in Fig. 3(c). We find that the G_{peak} value remains nearly constant with decreasing temperature. This weak metallic behavior for the conductance peak suggests that the peak position at which electrical field drives electrons drifting instead of hopping exhibits electronic states. In contrast, the $G_{\mathrm{min}\,1}$, $G_{\mathrm{min}\,2}$, and $G_{\mathrm{min\_tp20}}$ drastically decrease and show insulating behavior. The thermal activation gaps Δ for the $\nu = 0$ state can be estimated from Arrhenius fitting, $G \sim \exp(-\Delta/2k_BT)$, at varying B, as shown in Fig. 3(d). $\Delta_{\mathrm{min\text{-}tp20}}$ shows a linear dependence on B, consistent with previous experimental results obtained for graphene on h-BN [34]. $\Delta_{\mathrm{min}\,1}$ and $\Delta_{\mathrm{min}\,2}$ are scaling with $\sqrt{B}$. A $\sqrt{B}$ dependence for $\nu = 0$ in the Z-GNR is consistent with the theoretical models based on e-e interactions scaling with Coulomb energy scale $e^2/\varepsilon l_B$ [35], where is the dielectric constant and l_B is the magnetic length proportional to $1/\sqrt{B}$.

It has been shown above that magnetotransport measurements of Z-GNR show discernible features that are not observed for the nonzigzag GNR with a similar geometry. We assume that the observed conductance peak is related to the zigzag edge property. The temperature and magnetic

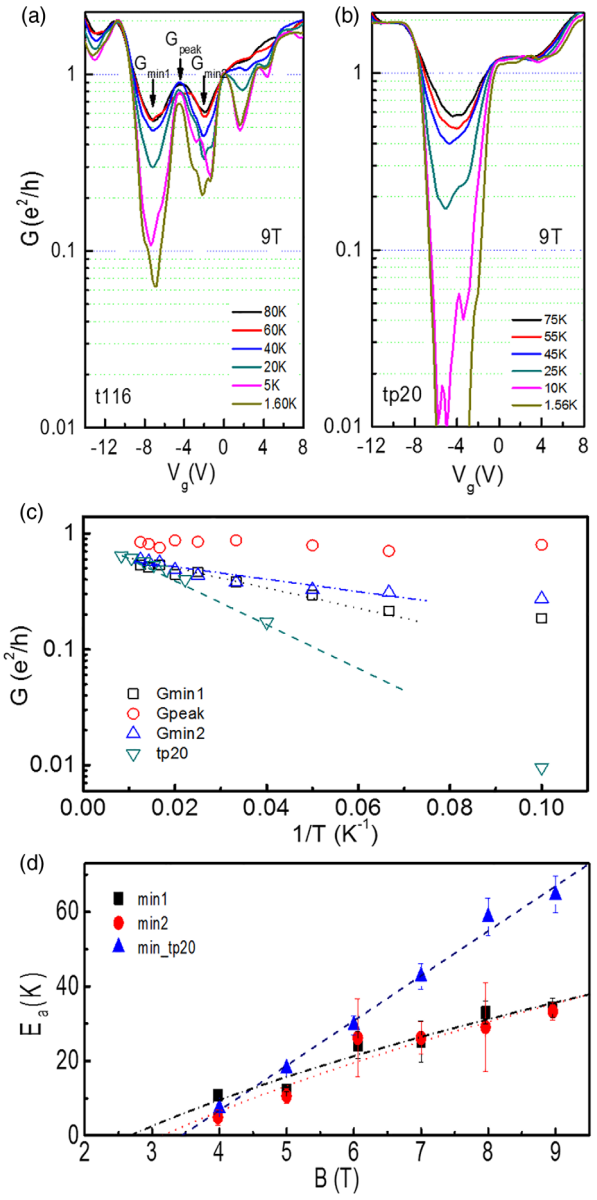

FIG. 3. Temperature dependence behavior of G_{peak}, $G_{\mathrm{min}\,1}$, and $G_{\mathrm{min}\,2}$. (a),(b) The typical transfer curves for #t116 and #tp20 at several temperatures $B = 9$ T. (c) T dependence of G_{peak}, $G_{\mathrm{min}\,1}$, and $G_{\mathrm{min}\,2}$. The straight lines are linear fits to the data at the high-temperature activation range. (d) Activation energy estimated by T dependence of $G_{\mathrm{min}\,1}$, $G_{\mathrm{min}\,2}$, and $G_{\mathrm{min}\,\_tp20}$ as a function of applied magnetic field B. The blue dashed line is fitted to B. The red dotted line and black dot-dashed line are fitted to $\sqrt{B}$.

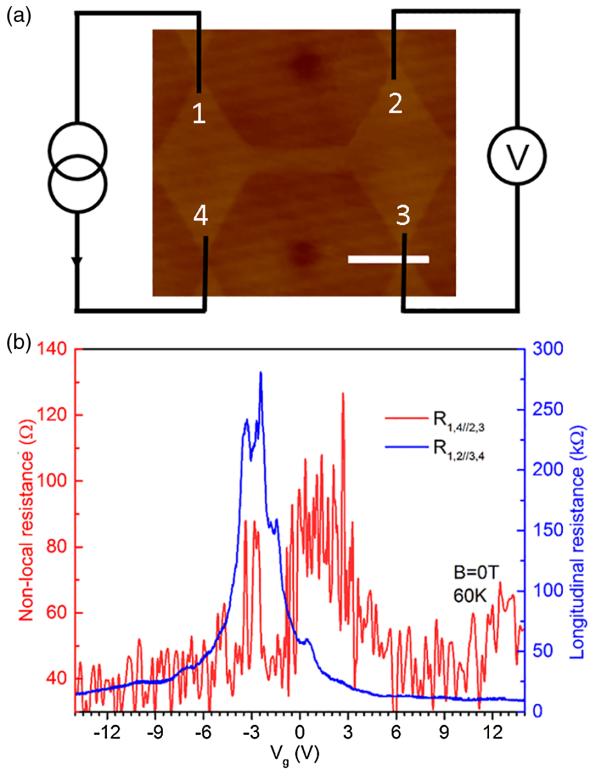

FIG. 4. Nonlocal measurement $(1,3//2,4)$ of Z-GNR. (a) AFM image of the typical Z-GNR/h-BN device ($l \sim 280$ nm, $w \sim 65$ nm) and the nonlocal measurement geometry; scale bar is 250 nm. (b) Nonlocal resistance (red curves) and longitudinal resistance (blue curve) measured in Z-GNR device.

field dependence of the conductance peak indicates that the zigzag edge can facilitate conduction. To evidence and isolate the edge conduction from bulk conduction, a nonlocal measurement for the Z-GNR at zero magnetic field is performed. As shown in Fig. 4, the electrical current was passed through the terminals 1 and 4 while detecting the voltage across terminals 2 and 3. Near the charge neutrality point (CNP) ($V_g \approx -3.0$ V), we observed an increase in the nonlocal resistance ($R_{1,4//2,3}$) at approximately $V_g \approx 1.2$ V. The position of the nonlocal voltage signal relative to the CNP, qualitatively consistent with edge conduction behavior, is in agreement with that of the magnetoconductance peak. When the Fermi level lies at the zigzag-energy band, electrons move along the edges (from 1 to 2 or from 3 to 4) and accumulate at the other terminal, thus generating a voltage potential. From the above STM characterization, we can see that etched edges can show a certain roughness. Hence, the edge conduction is likely affected by scattering from the atom steps or bulk carriers in such a channel length, which results in degradation of the nonlocal voltage amplitude.

We have already demonstrated the magnetotransport properties of graphene nanoribbons with zigzag edges and confirmed edge conduction through nonlocal measurement. It is expected that the origin of transport behavior observed for the zigzag edge is related to its electronic structure. We probed the electronic structure of hydrogen-etched zigzag edge of graphene on a $6H$-SiC(0001) substrate through scanning tunneling spectroscopy (STS) (Fig. 5). Figure 5(a) shows an atom-resolved STM image of the etched zigzag edges; the corresponding atomic lattice model for the top layer graphene with hydrogen termination is shown in Fig. 5(b). In differential conductance (dI/dV) spectra measurements [Fig. 5(c)] along the line perpendicular to the zigzag edge [green line in Fig. 5(a)], a peak appears (-6.0 meV) near the Fermi level at the zigzag edge, confirming the existence of a density of states (DOS). The intensity of this state drastically decreases when the tip moves into the interior of the top-layer graphene, as evidenced for the bulk electronic state of bilayer graphene (Fig. S4 [16]) and eventually disappears at a distance of $\sim$12.5 Å. Note that the localized state on the bottom graphene layer is not detectable even at a short distance of $\sim$9 Å from the edge. The amplitude of the DOS in Fig. 5(c) shows an exponential decay with distance from the zigzag edge, with the decay length

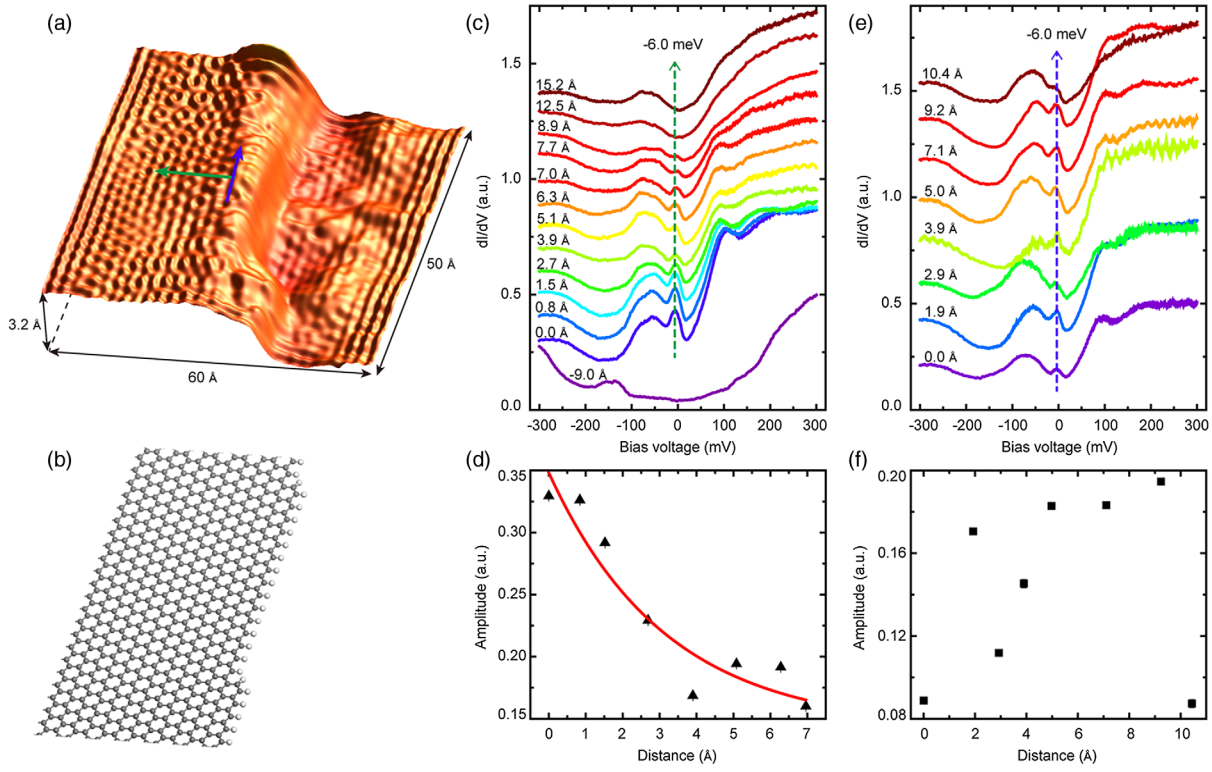

FIG. 5. Edge states at hydrogen-etched edge of graphene. (a) Atomically resolved STM topography ($V_s = -500$ mV, $I = 100$ pA, $T = 4.9$ K) shows the edge of the hydrogen-plasma etched graphene on $6H$-SiC(0001) substrate. (b) The atomic lattice model of the top-layer graphene shown in (a) (the gray ones and the white ones are carbon and hydrogen atoms) (c) dI/dV spectra measured along the green line in (a). (d) Solid triangles show the zigzag-edge-state amplitude extracted from (c) by Lorentz fitting, as a function of the distance from the zigzag edge, and red curve is the exponential decay fitting of the experimental data. (e) dI/dV spectra measured along the graphene edge, as the purple line shown in (a). (f) Solid squares show the zigzag-edge-state amplitude extracted from (e) by Lorentz fitting, indicating the amplitudes are uniform alone the edge. The spectra in (c) and (e) were measured with tip stabilized at $V_s = -500$ mV and $I = 100$ pA.

determined to be 3.2 Å [Fig. 5(d)]. Figure 5(e) shows the dI/dV spectra along the zigzag edge [the purple line in Fig. 5(a)], which indicate that the localized state exists at all sites of the edge and that the amplitude of DOS is almost homogeneous [Fig. 5(f)]. The peak localized at −6.0 meV is consistent with the reported results [20], indicating a high quality for the etched zigzag edges. Moreover, it has been previously demonstrated that the calculated bands for a freestanding ribbon and a supported ribbon are similar [20]. Because of the weak coupling between graphene and h-BN, the intrinsic electronic properties of graphene on h-BN are almost the same as those of freestanding graphene [36]. Note that only the rotational misaligned graphene/h-BN van der Waals heterostructure is considered here. Moreover, an edge state in epitaxially grown graphene/h-BN heterostructures on Cu has been previously probed by STS [37] and is in qualitative agreement with our results. It is reasonably proposed that a similar edge state exists at the hydrogen-etched zigzag edge of graphene on h-BN.

In our case, the width of the Z-GNR ranges from 60–120 nm. The band gap opening caused by antiferromagnetic spin-ordered edge states due to electron-electron interaction cannot occur when the Z-GNR is wider than 8 nm [13]. Since edge states decay exponentially into the bulk, they can be studied in much wider ribbons as states of semi-infinite ribbons. The states between two zigzag edges are uncoupled if the ribbon width is much larger than the decay length. Based on the reported inverse correlation between edge-state splitting induced by electron-electron interaction and the GNR width [38], the edge-state splitting is determined to be experimentally unresolvable for our Z-GNRs with a width ranging from 60–120 nm. In the case of a semi-infinite ribbon with pristine zigzag edges, the edge states occur at zero energy [4]. The electronic structure of the etched zigzag-edges in semi-infinite graphene can be utilized as a characteristic of the electronic structure of the etched Z-GNRs.

Here, we give a phenomenological description for how the zigzag-edge state influences magneto-transport behavior. In theory, zigzag-edged graphene has a nondispersive edge band at the CNP, which would have a localized edge state. However, in practical cases, the edge band is not strictly flat [2], which indicates the existence of delocalized electronic states. The small curvature of the quasiflat band prevents the electronic states at the edges from reaching a higher group velocity ($v_g \sim dE/dk$), which limits the conducting ability of the zigzag-edge state. Moreover, calculations considering the effect of edge defects via the inclusion of a periodic edge roughness indicate significant band opening, resulting a mid-gap-edge state [39]. When a magnetic field is applied perpendicular to graphene placed on h-BN, Landau levels will emerge. The observation of a nearly zero conductance plateau indicates the occurrence of a $\nu = 0$ broken symmetry state, which is related to the upshift (downshift) of electron (hole) $N = 0$ Landau level [29,34,40]. The linear dependence of the $\nu = 0$ activation gap on B in the control sample can be explained by the model predicting a linear dependence in which $\nu = 0$ is a spin-unpolarized ground state with an orbital origin [34]. For zigzag-edged graphene, the quasiflat edge bands are still located in the gap and are supposed to produce a conductance peak with $2e^2/h$ at the Landau filling $\nu = 0$. Experimentally, the $\sqrt{B}$ dependence for the $\nu = 0$ activation gap indicates a mechanism involving e-e interactions, different from the linear B-dependence mechanism. Theories have predicted that interacting electrons may have a suppression effect on conductance quantization in a perpendicular magnetic field [41]. Up to now, the original scenario of the $\nu = 0$ insulating state remains inconclusive. The transition of spin texture between the bulk $\nu = 0$ state and zigzag edge state needs both further experimental and further theoretical investigation.

The authors would like to thank Professor Feng Wang (Berkeley), Professor Jeffrey Bokor (Berkeley), Ting Cao (Berkeley), and Dr. Jon Gorchon (Lawrence Berkeley Lab) for useful discussions. This work was supported by the National Natural Science Foundation of China (NSFC, Grants No. 61325021 and No. 91223204), the "Strategic Priority Research Program (B)" (Grants No. XDPB0602 and No. XDB07010100) and the Key Research Program of Frontier Sciences (Grants No. OYZDB-SSW-SLH0004) of the Chinese Academy of Sciences. Y. Y. was supported by the MOST Project of China (No. 2014CB920903), the National Natural Science Foundation of China (Grants No. 11574029 and No. 11225418). W. W. is grateful to the financial support of the Hundred Talents Program of the Chinese Academy of Sciences.

S. W. and B. L. contributed equally to this work.

*Present address: Department of Electrical Engineering and Computer Sciences, University of California at Berkeley, Berkeley, California 94720, USA.

†To whom all correspondence should be addressed.
gyzhang@aphy.iphy.ac.cn

[1] A. H. Castro Neto, F. Guinea, N. M. R. Peres, K. S. Novoselov, and A. K. Geim, Rev. Mod. Phys. **81**, 109 (2009).
[2] N. M. R. Peres, F. Guinea, and A. H. Castro Neto, Phys. Rev. B **73**, 125411 (2006).
[3] C. Stampfer, J. Güttinger, S. Hellmüller, F. Molitor, K. Ensslin, and T. Ihn, Phys. Rev. Lett. **102**, 056403 (2009).
[4] K. Nakada, M. Fujita, G. Dresselhaus, and M. S. Dresselhaus, Phys. Rev. B **54**, 17954 (1996).
[5] L. Brey and H. A. Fertig, Phys. Rev. B **73**, 235411 (2006).
[6] A. H. Castro Neto, F. Guinea, and N. M. R. Peres, Phys. Rev. B **73**, 205408 (2006).
[7] Y.-W. Son, M. L. Cohen, and S. G. Louie, Nature (London) **444**, 347 (2006).
[8] Y.-W. Son, M. L. Cohen, and S. G. Louie, Phys. Rev. Lett. **97**, 216803 (2006).
[9] D. A. Abanin, P. A. Lee, and L. S. Levitov, Solid State Commun. **143**, 77 (2007).
[10] K. A. Ritter and J. W. Lyding, Nat. Mater. **8**, 235 (2009).

[11] P. Ruffieux *et al.*, Nature (London) **531**, 489 (2016).
[12] S. Wang, L. Talirz, C. A. Pignedoli, X. Feng, K. Mullen, R. Fasel, and P. Ruffieux, Nat. Commun. **7**, 11507 (2016).
[13] G. Z. Magda, X. Jin, I. Hagymasi, P. Vancso, Z. Osvath, P. Nemes-Incze, C. Hwang, L. P. Biro, and L. Tapaszto, Nature (London) **514**, 608 (2014).
[14] Z. Shi, R. Yang, L. Zhang, Y. Wang, D. Liu, D. Shi, E. Wang, and G. Zhang, Adv. Mater. **23**, 3061 (2011).
[15] R. Yang, L. Zhang, Y. Wang, Z. Shi, D. Shi, H. Gao, E. Wang, and G. Zhang, Adv. Mater. **22**, 4014 (2010).
[16] See Supplemental Material at http://link.aps.org/supplemental/10.1103/PhysRevLett.120.216601, for a description of the sample fabrication, characterization, and data analysis.
[17] S. Wu, R. Yang, D. Shi, and G. Zhang, Nanoscale **4**, 2005 (2012).
[18] J. Lin, L. Guo, Y. Jia, R. Yang, S. Wu, J. Huang, Y. Guo, Z. Li, G. Zhang, and X. Chen, Appl. Phys. Lett. **104**, 183102 (2014).
[19] X. Zhang *et al.*, ACS Nano **7**, 198 (2013).
[20] Y. Y. Li, M. X. Chen, M. Weinert, and L. Li, Nat. Commun. **5**, 4311 (2014).
[21] Y. Niimi, T. Matsui, H. Kambara, K. Tagami, M. Tsukada, and H. Fukuyama, Phys. Rev. B **73**, 085421 (2006).
[22] T. Kondo, Y. Honma, J. Oh, T. Machida, and J. Nakamura, Phys. Rev. B **82**, 153414 (2010).
[23] Y. Kobayashi, K.-i. Fukui, T. Enoki, K. Kusakabe, and Y. Kaburagi, Phys. Rev. B **71**, 193406 (2005).
[24] C. R. Dean *et al.*, Nat. Nanotechnol. **5**, 722 (2010).
[25] R. Decker, Y. Wang, V. W. Brar, W. Regan, H.-Z. Tsai, Q. Wu, W. Gannett, A. Zettl, and M. F. Crommie, Nano Lett. **11**, 2291 (2011).
[26] G. Wang *et al.*, Appl. Phys. Lett. **109**, 053101 (2016).
[27] X. Wang, Y. Ouyang, L. Jiao, H. Wang, L. Xie, J. Wu, J. Guo, and H. Dai, Nat. Nanotechnol. **6**, 563 (2011).
[28] J. Bai, R. Cheng, F. Xiu, L. Liao, M. Wang, A. Shailos, K. L. Wang, Y. Huang, and X. Duan, Nat. Nanotechnol. **5**, 655 (2010).
[29] A. F. Young, J. D. Sanchez-Yamagishi, B. Hunt, S. H. Choi, K. Watanabe, T. Taniguchi, R. C. Ashoori, and P. Jarillo-Herrero, Nature (London) **505**, 528 (2014).
[30] D.-K. Ki and A. F. Morpurgo, Phys. Rev. Lett. **108**, 266601 (2012).
[31] F. Molitor, C. Stampfer, J. Güttinger, A. Jacobsen, T. Ihn, and K. Ensslin, Semicond. Sci. Technol. **25**, 034002 (2010).
[32] J. R. Williams, D. A. Abanin, L. DiCarlo, L. S. Levitov, and C. M. Marcus, Phys. Rev. B **80**, 045408 (2009).
[33] D. A. Abanin and L. S. Levitov, Phys. Rev. B **78**, 035416 (2008).
[34] A. F. Young, C. R. Dean, L. Wang, H. Ren, P. Cadden-Zimansky, K. Watanabe, T. Taniguchi, J. Hone, K. L. Shepard, and P. Kim, Nat. Phys. **8**, 550 (2012).
[35] K. Yang, Solid State Commun. **143**, 27 (2007).
[36] H. Sadeghi, S. Sangtarash, and C. Lambert, Physica (Amsterdam) **82E**, 12 (2016).
[37] B. Hwang *et al.*, Sci. Rep. **6**, 31160 (2016).
[38] C. Tao *et al.*, Nat. Phys. **7**, 616 (2011).
[39] R. Hassan, J. Phys. Condens. Matter **23**, 382203 (2011).
[40] K. Nomura and A. H. MacDonald, Phys. Rev. Lett. **96**, 256602 (2006).
[41] A. A. Shylau, I. V. Zozoulenko, H. Xu, and T. Heinzel, Phys. Rev. B **82**, 121410 (2010).